Solvated Electron Pairing with Earth Alkaline Metals in THF. 1. Formation and Structure of the Pair with Divalent Magnesium

F. Renou, M. Mostafavi,* P. Archirel,* L. Bonazzola, and P. Pernot

Laboratoire de Chimie Physique, CNRS UMR 8000, Université Paris-Sud, Centre d'Orsay, Bât. 349. 91405 ORSAY Cedex, France

Received: July 15, 2002; In Final Form: December 13, 2002

The reactivity of a solvated electron with Mg^{II} salts in THF is investigated by pulse radiolysis. With magnesium chloride, no reaction is observed, but when magnesium perchlorate is used, the solvated electron reacts to form a species absorbing in the near-infrared. Conductivity measurements show that neither $MgCl_2$ nor $Mg(ClO_4)_2$ is dissociated in THF. Quantum chemical calculations show that the difference in behavior between the two salts can be traced back to the electron affinities of the solutes in the gas phase. The solvated electron forms a stable pair only with magnesium perchlorate. The structure of this pair is proposed. The rate constants of the reactions and the extinction coefficients of the different species involved in the formation and decay of the pair are determined with a probabilistic global analysis method of the time-resolved absorbance signals.

Introduction

Since the 1960s, the reduction of metal cations in solution by solvated electrons has been studied by pulse radiolysis.[1] In some cases, unusual valence states are observed from their transient optical absorption. Their reactivity and the reaction mechanisms are established by following the kinetics of formation and decay in solutions containing other solutes. Some metal cations, such as alkaline and alkaline earth cations, cannot be reduced by hydrated electrons in water. Nevertheless, the reduction of alkaline metal cations by solvated electrons in less polar solvents was studied during the 1970s.[2] The alkaline earth group was studied by pulse radiolysis in alcohol solutions only. An ion pairing of solvated electrons affecting the absorption spectra was observed in ethanol.[3]

In water, γ-radiolysis studies showed that the reaction between a hydrated electron and Mg^{2+} does not occur because the value of the redox potential of Mg^{2+}/Mg^{+} is lower than that of the hydrated electron.[4] We recently confirmed this result by observing the decay of solvated electrons in the presence of different Mg^{2+} concentrations.[5] Indeed, the observed kinetics were not affected by the presence of Mg^{2+}, even at concentrations as high as 10^{-2} mol dm^{-3}.

Magnesium is an interesting system because of the importance of its reactivity in organic chemistry. As a precursor of the Grignard compounds, RMgX (R: alkyl radical and X: halogen atom), the magnesium metal powder is generally assumed to dissolve and eventually to form divalent ions in solution during the reaction with RX compounds. But the nature of transient magnesium states in the oxidation process of metal powder is still unknown. In particular, the formation mechanism of the Grignard compounds used for over a century[6] has not yet been established unambiguously.[7,8] This raises questions about the possible role of monovalent magnesium, which is formed through the first monoelectronic oxidation of the metal in organic solutions by RX during the synthesis of Grignard compounds.

In a preliminary paper, we recently reported a reaction between a solvated electron and Mg^{II} in different weakly polar solvents such as ethers:

$$Mg^{II} + e_s^- \rightarrow P \qquad (1)$$

We used only magnesium perchlorate, $Mg(ClO_4)_2$, as a solvated electron scavenger. The rate constant of reaction 1 was estimated to be around 10^{10} dm^3 mol^{-1} s^{-1} in diethyl ether and tetrahydrofuran. Because we did not identify the structure of the magnesium cation in solution, Mg^{II} in reaction 1 stands for a dissociated or an undissociated form of the salt. We showed that the reduction of the divalent magnesium by a solvated electron in diethyl ether and tetrahydrofuran leads to the formation of a species absorbing in the near-infrared. We suggested that the observed species is either the monovalent magnesium ion Mg^{I} or a solvated electron−ion pair (Mg^{II}, e_s^-).[5]

In the present work, we study reaction 1 in more detail by identifying the structure of Mg^{II} in solution for two different salts and by determining the nature of the product. For that purpose, we carried out conductivity measurements of THF solutions containing one of the two magnesium salts $Mg(ClO_4)_2$ or $MgCl_2$. Then, we followed the reactivity of the solvated electron with these two salts in THF by nanosecond pulse radiolysis. The kinetics data are analyzed by a probabilistic global method to assess the identifiability of the kinetics parameters (formation and decay rate constants and absorption optical properties). The experimental results are supported by ab initio calculations, enabling to identify the nature of the product of reaction 1 and to determine the thermodynamics of this reaction.

Experimental and Theoretical Methods

1. Experimental. Tetrahydrofuran (THF) of 99.5% purity was purchased from Fluka. THF was distilled in the presence of metallic sodium under an argon atmosphere to remove water

* Corresponding authors. Mehran Mostafavi from the group of electron transfer in condensed medium (e-mail: mehran.mostafavi@lcp.u-psud.fr) and Pierre Archirel from the theoretical chemistry group (e-mail: pierre.archirel@lcp.u-psud.fr).

10.1021/jp0216124 CCC: $25.00
Published on Web 02/19/2003

and oxidizing agents. The alkaline earth perchlorates and chlorides, purchased from Aldrich, were used as received.

A CDM 210 radiometer Copenhagen was used for the conductivity measurements. The measurements range was from 0.01 to 5.99 μS cm^{-1} with different frequencies defined for specific conductivity domain. The cell constant is calibrated before each experiment with solutions of KCl, and the value is around 0.88 cm^{-1}. The two electrodes are made with platinum and do not react with THF. All of the conductance measurements are performed at room temperature. The conductivity of the pure solvent was below the detection threshold.

The pulse radiolysis setup has been described elsewhere.[9] Electron pulses (3-ns duration) were delivered by a Febetron 706 accelerator (600-keV electron energy) to samples contained in a quartz suprasil cell through a thin entrance window (0.2 mm) having an optical path length (1 cm) perpendicular to the electron beam. The cell was deaerated via nitrogen flow before the experiment. The solution was changed after each pulse. The optical absorption of the transient species was recorded by means of a classical xenon lamp, monochromator, and photomultiplier or diode setup with a sensitive surface of 1-mm radius. The spectrophotometer detection system had an overall rise time of 3.7 ns in the visible spectral domain and 12 ns in the infrared domain. The reported values of the transient optical density are averaged over at least 10 measurements.

2. Data Analysis of Transient Signals. Transient absorbance signals $A(t, \lambda)$ are expressed as

$$A(t, \lambda) = \sum_{i=1}^{N} c_i(t, K)\, \epsilon_i(\lambda) \qquad (2)$$

where t is the time, λ is the spectral coordinate, ϵ_i is the extinction coefficient of species i, c_i is the instantaneous concentration, and K represents the set of parameters involved in the kinetics model.

2.1. Simulation of Reaction Kinetics. The concentrations of transient species (c_i) are obtained by numerical simulation of the rate equations corresponding to a set of chemical reactions. In this work, the pulse duration is short compared to the monitored processes, and we do not explicitly take the dose rate into account in the equations. Initial conditions are rather specified through the "initial" concentrations (i.e., just after the pulse) of the precursor species (solvated electron, radicals, etc.). The resulting set of coupled nonlinear ordinary differential equations is integrated with the LSODA routine, which adapts automatically to stiff or nonstiff conditions.[10]

2.2. Parameter Identification. In pulsed radiolysis experiments, the unknown parameters usually include spectral properties of transient species and reaction rates. Under our experimental conditions (in the absence of the exact dose value and radiolytic yields), we also have to consider the initial concentrations of the precursor species (solvated electron, radicals, etc.) as unknown. The identification of these parameters is known to be problematic,[11,12] and it was expected that some parameters could not be identified.[13] This state can be improved to some extent with a global analysis strategy (i.e., simultaneous analysis of complementary experiments[14]), and we systematically use this approach in the present work. For convenience, we will distinguish global parameters involved in all of the analyzed experiments from local parameters related to a single signal.

We address the identifiability issue with a *practical* identification method based on probabilistic (Bayesian) data analysis.[15−19] Such a method is also used, for instance, in environmental modeling[20] and biokinetics.[21,22] It is based on stochastic sampling by Markov chains[23−25] of the posterior probability density function (pdf), $p(u|D)$, in the space of parameters u, for a given data set D. This method does not focus only on the best-fit solution but also on the set of parameters giving an acceptable fit, considering the uncertainty of the analyzed data. Details of the method are given in the Appendix.

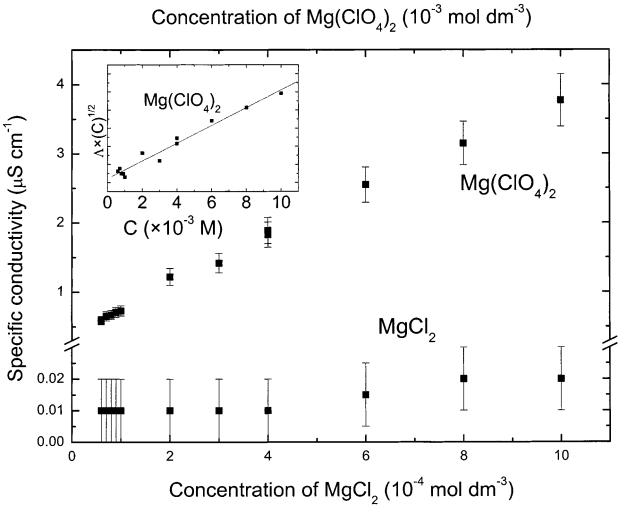

Figure 1. Specific conductivity of $MgCl_2$ and $Mg(ClO_4)_2$ in THF. Inset: fitting $\Lambda \times C^{1/2} = f(C)$ according to Fuoss−Kraus theory.

3. ab Initio Calculations for Structure Determination. The two neutral solutes—magnesium chloride, $MgCl_2$, and magnesium perchlorate, $Mg(ClO_4)_2$—in solution in THF are investigated with the help of SCF and DFT methods. We have considered explicitly the first solvation shell, which implies the treatment of up to four THF molecules. Since the systems are rather large, we have used the following strategy in two steps:

(1) geometry optimization of the THF-dressed solute in vacuum at the SCF level with a conventional 6-31G* basis set; and

(2) single-point DFT/B3LYP calculations at the SCF optimized geometry, including the field of the remaining solvent with the Onsager method. This method uses a spherical cavity that is well adapted to our systems, thanks to the first shell of THF molecules. We have compared the Onsager and polarized continuum medium (PCM) methods for ClO_4^- and have found that the Onsager method underestimates the solvation free energy by less than 10%.

We use the same strategy for the corresponding anions ($MgCl_2^-$ and $Mg(ClO_4)_2^-$) with a basis set for Mg augmented with two s, p, d, and f Gaussians having exponents of 0.02 and 0.01. These exponents have been obtained from the last exponent of the standard basis set (0.04) and a decreasing geometric law of factor 2. All of the calculations have been carried out with the Gaussian 98 program package.[26]

Results and Discussion

1. Structure of Magnesium Salts in THF. The only reported data on the conductivity of $Mg(ClO_4)_2$ concern very highly concentrated saturated solutions,[27] whereas the relevant concentration range for our experiments is from 6×10^{-4} to 10^{-2} mol dm^{-3} (i.e., below the solubility threshold). Therefore, we performed conductometric studies of solutions containing small concentrations of magnesium pechlorate or magnesium chloride in THF. The dependence of the conductivity on the concentration of the salts is reported in Figure 1. The specific conductivity, σ, of the $MgCl_2$ solutions is very low, close to the detection threshold, and remains approximately the same at any concen-

tration from 6×10^{-4} to 10^{-2} mol dm^{-3}. In contrast, the specific conductivity of magnesium perchlorate solutions increases with the concentration of the salt from 0.5 to 3.75 μS cm^{-1} for 6×10^{-4} to 10^{-2} mol dm^{-3}, respectively.

These results are explained by a dissociation equilibrium similar to the one De Groof and co-workers proposed for magnesium tetraphenylboron in THF.[28] Because of the low polarity of the solvent, the total dissociation of magnesium perchlorate is neglected.

$$MgClO_4^+ + ClO_4^- \rightleftharpoons Mg(ClO_4)_2 \qquad (3)$$

Experimental data could not be fitted by the Onsager law, and because equilibrium 3 is similar to that of a monovalent system, because we take into account only the dissociation of one perchlorate, we can use the Fuoss−Kraus theory of the triple ion.[29] This method has also been applied to the study of the dissociation of sodium perchlorate in THF.[31] According to the Fuoss−Kraus theory of the triple ion, the molar conductivity $\Lambda = \sigma/C$ is related to the association constant K_3, the limiting conductance of the ionic couple Λ_0, the association constant of the triple-ion equilibrium K_T, and the limiting conductance of the ionic species Λ_T^0 involved in the triple-ion equilibrium through the following equation:

$$\Lambda\sqrt{C} = \frac{\Lambda_0}{\sqrt{K_3}} + \frac{\Lambda_T^0 K_T}{\sqrt{K_3}} \times C \qquad (4)$$

where $K_3 = [Mg(ClO_4)_2]/[MgClO_4^+][ClO_4^-]$ and K_T corresponds to the triple-ion equilibrium

$$Mg(ClO_4)_2 + ClO_4^- \rightleftharpoons Mg(ClO_4)_3^- \qquad K_5 \qquad (5)$$

$$Mg(ClO_4)_2 + MgClO_4^+ \rightleftharpoons Mg_2(ClO_4)_3^+ \qquad K_6$$
$$K_T = K_5 \approx K_6 \qquad (6)$$

The notion of a triple ion in our case means that there is a possibility of association between one free ionic species ($MgClO_4^+$ or ClO_4^-) and the neutral species $Mg(ClO_4)_2$. Consequently, the triple ion is either $Mg(ClO_4)_3^-$ or $Mg_2(ClO_4)_3^+$. Without information on K_5 and K_6, Fuoss and Kraus make the approximation that the two equilibrium constants have similar values, which they justify by considering an average ion size.

The function $\Lambda\sqrt{C} = f(C)$ is reported in the inset of Figure 1. The best linear fit gives an intercept of 7.2×10^{-5} S cm$^{1/2}$ mol$^{-1/2}$ and a slope of 4.9×10^{-6} S cm$^{7/2}$ mol$^{-3/2}$. In THF, the value of the limiting conductance of ClO_4^- is known to be $\lambda_0^- = 119.5$ S cm^2 mol^{-1}.[30] We assume the value of Λ_0 for $MgClO_4^+$, ClO_4^- ($\Lambda_0 = \lambda_0^+ + \lambda_0^-$), to be around 200 S cm^2 mol^{-1}. For the triple-ion equilibrium, using $\Lambda_T^0 = {}^1/_3\Lambda^0 = 67$ S cm^2 mol^{-1}, we obtain $K_T = 193$ M^{-1}. Therefore, we can estimate the association constant using eq 4 as $K_3 \approx 7 \times 10^7$ mol^{-1} dm^3. This value is in agreement with those obtained for other perchlorate salts in THF: 9.9×10^7, 1.7×10^6, and 4.8×10^7 M^{-1} for $NaClO_4$,[31] Bu_4NClO_4,[32] and $LiClO_4$,[33] respectively. Eventually, we can conclude that even in the case of $Mg(ClO_4)_2$ solutions there is no noticeable dissociation of the salt in THF. Even if we consider a large uncertainty for the value of $\lambda(MgClO_4^+)$, the result is not significantly changed: the main species in solution is the neutral form $Mg(ClO_4)_2$. For example, if we divide the value of $\lambda(MgClO_4^+)$ by 2 (i.e., $\lambda(MgClO_4^+) = 40$ S cm^2 mol^{-1}), then we obtain an association constant of K_3 that is equal to 4.9×10^7 dm^3 mol^{-1}.

Indeed, it has been shown previously that ionic salts in weakly polar solvents are weakly dissociated and that their neutral form is actually an ion pair.[34] The ion pair can be in a single cavity, or several layers of solvent can be present between the two ions to form their own cavities. But the distance between them remains short, and important conductivity cannot be observed. Not only for $MgCl_2$ but also for magnesium perchlorate, the neutral form of the salt (i.e., $Mg(ClO_4)_2$) is largely the most abundant species in THF solution (e.g., for a concentration of 10^{-3} mol dm^{-3} $Mg(ClO_4)_2$, less than 3.8×10^{-6} mol dm^{-3} of the salt is dissociated). The lack of information on K_5 and K_6 has no great importance since the dissociation is very weak and the concentration of ionic species, whatever their form, is too low to consider a possible reaction with solvated electrons.

2. Reactivity of the Solvated Electron with Magnesium Salts in THF. Considering the expected parameters' identifiability problems, we proceed by analyzing sequentially the elementary reactions involved in the system. The determination of the kinetic and spectroscopic properties of the solvated electron in THF appears to be the keystone of the whole process. Moreover, it is used to illustrate the probabilistic global analysis method on a rather simple problem.

2.1. Decay of the Solvated Electron in Pure THF. In the absence of any solute, the decay of the solvated electron is very fast, and it is attributed to the following reaction:

$$e_s^- + THF^+ \rightarrow \text{products} \qquad (7)$$

THF^+ in reaction 7 stands for the hole or radicals formed in the solution by the electron pulse. The nature of this species is not clearly established, but it is well known that the hole and radicals react with the solvated electron.[35] We performed several measurements of the decay of the solvated electron by changing the dose per pulse. In Figure 2, we show only one of these decays.

Considering that the absorbance of the hole is negligible at 1000 nm, the expression of the total absorbance includes four unknown parameters: the initial concentrations $[e_s^-]_0$ and $[THF^+]_0$, the absorption coefficient of e_s^- ($\epsilon_{e_s^-}$), and the rate constant k_7. The analytical expression[36] of the absorbance observed through an optical length l (1 cm) for reaction 7

$$A(t, \lambda = 1000\ \text{nm}) = l\epsilon_{e_s^-} \frac{[e_s^-]_0([THF^+]_0 - [e_s^-]_0)}{[THF^+]_0 \exp(-([e_s^-]_0 - [THF^+]_0)k_7 t) - [e_s^-]_0} \qquad (8)$$

reveals that a simple rescaling of one of the parameters can be exactly compensated by a reciprocal scaling of the other parameters (nonlinear couplings between parameters). Scatter plots of a Markov chain for this system unambiguously exhibit this coupling structure (Figure 3). For example, there is a linear coupling between k_7 and $\epsilon_{e_s^-}$ and a nonlinear coupling between the latter and $[e_s^-]_0$. Without external (a priori) information, the parameters are unidentifiable (i.e., the best fit of the experimental signal by this model can be achieved at an infinite number of points in parameter space). This is an obvious case of structural unidentifiability.[13] Note that fixing the value of any of the parameters would make this model structurally identifiable. With that intent, we estimated that $\epsilon_{e_s^-} = (1.0 \pm 0.1) \times 10^4$ mol^{-1} dm^3 cm^{-1} at 1000 nm from a transient absorption spectrum of the solvated electron in THF that has been reported in the literature.[37]

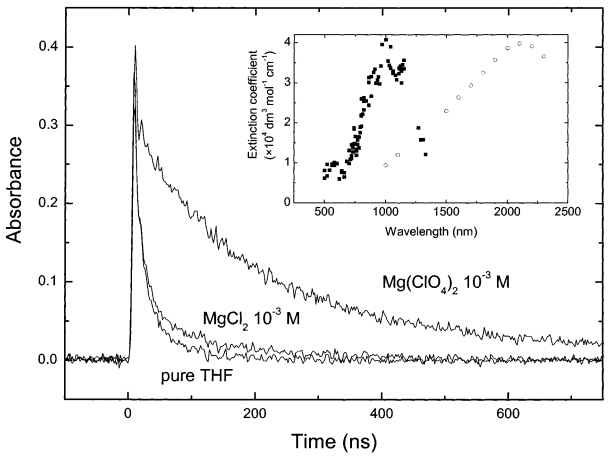

Figure 2. Absorption signals at 1000 nm in THF for pure solvent, $MgCl_2$, and $Mg(ClO_4)_2$. Inset: absorption spectrum of the product of the reaction $Mg(ClO_4)_2 + e_s^-$ (■) and of the solvated electron e_s^- (○).

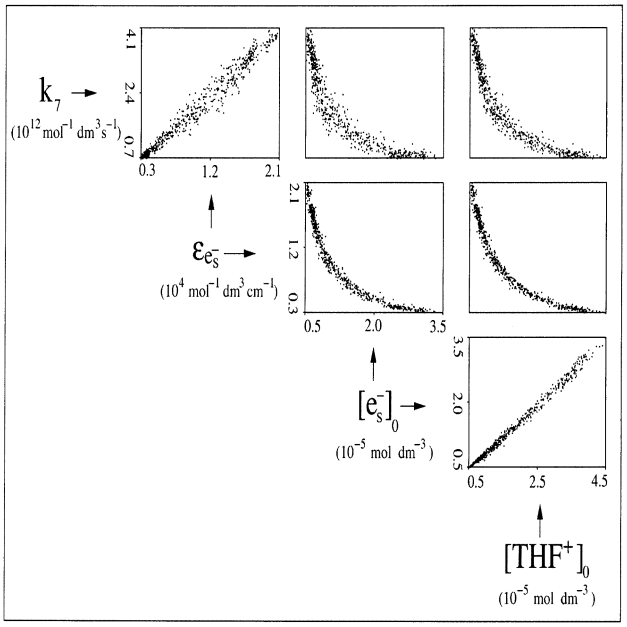

Figure 3. Correlation between different parameters ($\epsilon_{e_s^-}$, k_7, $[e_s^-]_0$, and $[THF^+]_0$) issued from the global analysis of the solvated electron transient absorbance at 1000 nm in pure THF: scatter plot matrix for four parameters extracted from a Markov chain with 20 parameters. The pairwise scatter plots are represented in an upper triangular matrix whose rows and columns are indexed by the parameter names specified along the diagonal. The two global parameters of the model (rate constant k_7 and absorption coefficient $\epsilon_{e_s^-}$) are reported along with a representative single pair of local parameters (initial concentrations $[e_s^-]_0$ and $[THF^+]_0$) corresponding to one of the nine analyzed signals.

We treated a set of nine decays corresponding to different values of the dose per pulse. The global analysis requires 20 parameters: k_7, $\epsilon_{e_s^-}$ as global parameters, and nine pairs of initial concentrations for e_s^- and THF^+ (local parameters). Prior and posterior marginal distributions for the parameters, extracted from a Markov chain of 10^6 steps, are reported in Table 1 and Figure 4. All parameters except $\epsilon_{e_s^-}$, are well identified and present normal marginal posterior pdf's. The marginal posterior distribution function (pdf) of $\epsilon_{e_s^-}$ is identical to its prior pdf (the studied data do not provide any information on this parameter), and $\epsilon_{e_s^-}$ remains undetermined between 9000 and 11 000 mol^{-1} dm^3 cm^{-1} at 1000 nm. The estimated value $k_7 = (1.9 \pm 0.2) \times 10^{12}$ mol^{-1} dm^3 s^{-1} for the rate constant is in good agreement with the reported value 2×10^{12} mol^{-1} dm^3 s^{-1}.[35] It is also noteworthy that reasonable values are recovered for the initial concentrations of solvated electrons and holes, supporting the validity of this effective model. In all cases, the initial concentration of the hole is slightly higher than that of the solvated electron.

TABLE 1: Estimations of Parameters from the Analysis of a Set of Nine Decays Observed at 1000 nm in Pure THF[a]

	prior	posterior
k_7 (10^{12} mol^{-1} dm^3 s^{-1})	[5×10^{-2}, 5]	1.9 ± 0.2
$\epsilon_{e_s^-}$ (10^4 mol^{-1} dm^3 cm^{-1})	[0.9, 1.1]	[0.9, 1.1]
$[e_s^-]$ (10^{-5} mol dm^{-3})	[10^{-1}, 10]	1.1 ± 0.1
$[THF^+]$ (10^{-5} mol dm^{-3})	[10^{-1}, 10]	1.4 ± 0.1

[a] The initial concentrations were reported only for one of the signals. The prior pdf's are log-uniform distributions (noted [a, b]). Except for $\epsilon_{e_s^-}$, the posterior pdf's are normally distributed, and we report here their mean value and standard deviation.

2.2. Decay of Solvated Electrons in the Presence of Magnesium Salts. Figure 2 shows the signals obtained 1000 nm after the electron pulse in pure THF and in solutions of $MgCl_2$ and $Mg(ClO_4)_2$ at the same concentration. The signals for the pure solvent and in the presence of $MgCl_2$ at 10^{-3} mol dm^{-3} (near its maximum of solubility in THF) are very similar. For $Mg(ClO_4)_2$, the signal is very different: the apparent decay after 20 ns is slowed with respect to the decay in pure THF or in the presence of $MgCl_2$. This shows clearly that the reactivity of the two salts is different. With $Mg(ClO_4)_2$, the product of reaction 1 is generated during the pulse and disappears spontaneously. On the contrary, with chloride salt, only the absorbance of the solvated electron is observed, indicating that the reaction between the solvated electron and $MgCl_2$ does not occur.

We note that $Mg(ClO_4)_2$ is very hygroscopic and that water molecules are probably present in the studied solutions. The solvated electron does not react with water molecules, but we cannot exclude a reaction of the hole (THF^+) with H_2O molecules. Nevertheless, because our kinetic model is based on an effective concentration of THF^+, which is treated as a free parameter, this effect is taken into account effectively.

In section 1, we showed that $Mg(ClO_4)_2$ and $MgCl_2$ at 10^{-3} mol dm^{-3} are solvated in their neutral forms. Therefore, the difference in reactivity with the solvated electron cannot be explained from the difference in the dissociation of the two salts in THF. Moreover, the analysis of the kinetics for different concentrations of $Mg(ClO_4)_2$ shows that the reaction of the solvated electron with the dissociated form of the salt, $MgClO_4^+$, cannot be considered. Figure 5 is a scatter plot of a Markov chain for Mg^{II} concentration and k_1. The scatter plot indicates that, for example, for a Mg^{II} concentration of about 4×10^{-6} mol dm^{-3} the best fit of the decays is obtained with k_1 greater than 2.5×10^{12} mol^{-1} dm^3 s^{-1}. According to the conductometric measurements, the concentration of the ionic species of divalent magnesium (i.e., $MgClO_4^+$) is in all cases less than 3.8×10^{-6} mol dm^{-3}. If we were to attribute the decay of the solvated electron to a reaction with $MgClO_4^+$ through reaction 1, then the rate constant of the reaction should be considered to be at least 2.5×10^{12} mol dm^{-3} s^{-1}. Such a rate constant would be well over the diffusion-limited rate constant in THF, which is less than 10^{12} mol dm^{-3} s^{-1}. The observed kinetics of the solvated electron and the product formation could be fitted only when the concentration of the metal cation is considered to be higher than 10^{-3} mol dm^{-3}. Therefore, reaction 1 with the solvated electron occurs with the neutral form of the metal cation (i.e., Mg^{II} stands for $Mg(ClO_4)_2$).

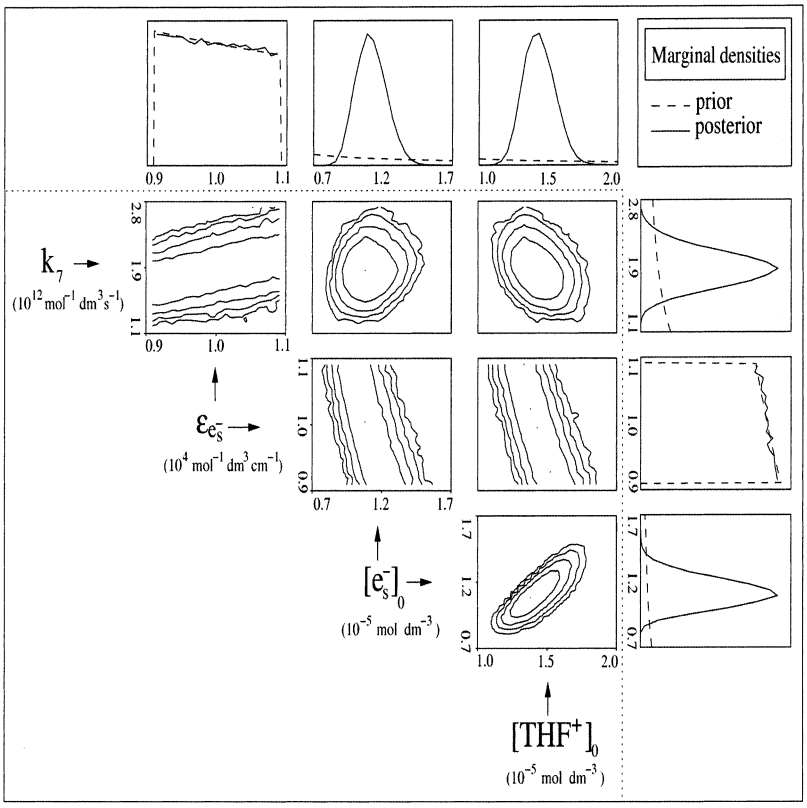

Figure 4. Marginal densities of the parameters ($\epsilon_{e_s^-}$, k_7, $[e_s^-]_0$, and $[THF^+]_0$) issued from the global analysis of the solvated electron transient absorbance at 1000 nm in pure THF: marginal density plot matrix for the same four parameters as in Figure 3 but with different prior information (see text). The pairwise marginal densities are reported in the inner triangular matrix (cf. Figure 3) as logarithmically spaced isodensity contour plots (in arbitrary units). The one-parameter marginal prior (- -) and posterior (—) densities are displayed along the margins of the matrix and are also indexed by the corresponding diagonal label.

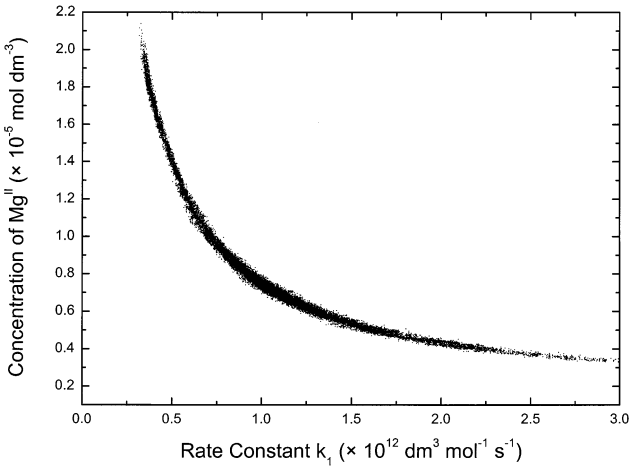

Figure 5. Correlations between k_7 and $[Mg^{II}]_0$ issued from the global analysis of the solvated electron transient absorbance at 1000 nm in pure THF shown by a scatter plot extracted from a Markov chain performed for the analysis of reactions 1, 7, 9, and 10.

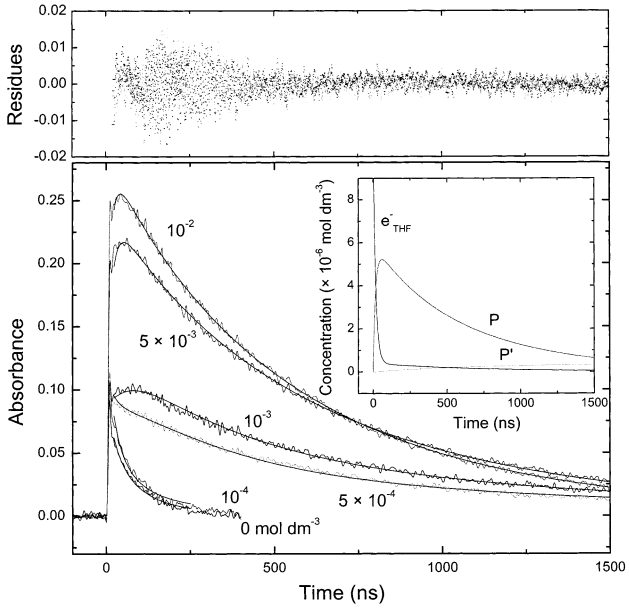

Figure 6. Lower graph: absorption signals at 1000 nm for THF solutions of different concentrations of $Mg(ClO_4)_2$. Inset: time evolution of the concentrations of e_s^-, P, and P′ obtained from the fit of the signal for a 10^{-3} mol dm^{-3} $Mg(ClO_4)_2$ concentration. Upper graph: residues from the best fit of all of the signals.

From pulse radiolysis measurements of the absorbance at different wavelengths in the presence of $Mg(ClO_4)_2$, we established more precisely than previously the absorption spectrum of the product (Figure 2 inset). By comparing to the spectrum obtained in our previous study,[5] we confirmed the presence of a shoulder around 1150 nm. The discontinuity of the spectrum near 1200 nm is due to the high absorption of THF. For comparison, we report the spectrum of the solvated electron in pure THF.[37]

In Figure 6, we reported the effect of the concentration of $Mg(ClO_4)_2$ on the kinetics observed at 1000 nm. In the absence of the solute or with a low concentration (10^{-4} mol dm^{-3}), we observe only a fast decay, achieved at 200 ns. For higher concentrations, the shape of the signal changes dramatically. First we observe an increase in the absorbance during 40 ns, followed by a slow decay. Note that the signals for concentra-

TABLE 2: Estimations of the Parameters Resulting from the Probabilistic Analysis of the Transient Signal of Figure 6[a]

	prior	posterior		
		$\epsilon_{e_s^-} = 9 \times 10^3$ $k_7 = 1.75 \times 10^{12}$	$\epsilon_{e_s^-} = 10^4$ $k_7 = 1.9 \times 10^{12}$	$\epsilon_{e_s^-} = 1.1 \times 10^4$ $k_7 = 2.12 \times 10^{12}$
k_1 (10^9 mol^{-1} dm^3 s^{-1})	[10^{-1}, 10^3]	6.2 ± 0.3	6.2 ± 0.2	6.3 ± 0.2
k_9 (10^6 s^{-1})	[10^{-3}, 10^2]	3.9 ± 0.1	3.8 ± 0.1	3.8 ± 0.1
k_{10} (s^{-1})	[10^2, 10^6]	[10^2, 10^6]	[10^2, 10^6]	[10^2, 10^6]
ϵ_P (10^4 mol^{-1} dm^3 cm^{-1})	[10^{-3}, 5]	3.6 ± 0.1	4.1 ± 0.1	4.3 ± 0.1

[a] See Table 1 for notation. The values of $\epsilon_{e_s^-}$ and k_7 are given in mol^{-1} dm^3 cm^{-1} and mol^{-1} dm^3 s^{-1}, respectively.

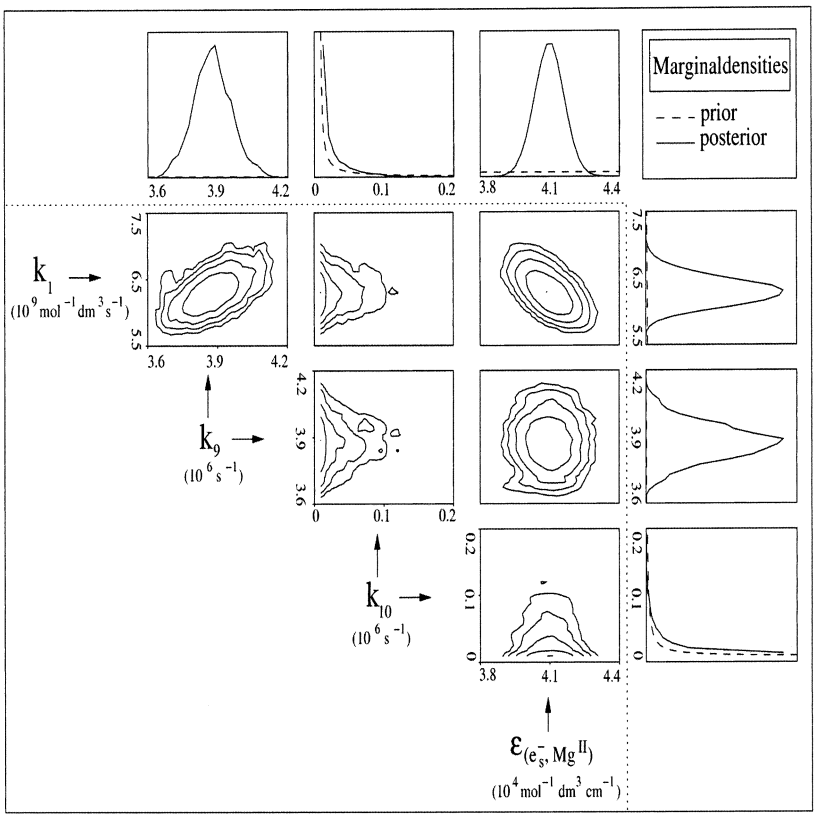

Figure 7. Global analysis of transient absorbance at 1000 nm in THF corresponding to the signals reported in Figure 6: marginal density plot matrix for four global parameters extracted from a Markov chain with 19 parameters.

tions of 5×10^{-3} mol dm^{-3} and 10^{-2} mol dm^{-3} are not parallel and cross around 800 ns (Figure 6).

Reaction 1 is reversible:

$$P \rightarrow e_s^- + Mg^{II} \qquad (9)$$

Reactions 1, 7, and 9 constitute the simplest mechanism for the observed kinetics. This mechanism has also been proposed for the solvated electron pairing with alkaline cations in THF.[2,35] In our preliminarily paper, we analyzed signals at times shorter than 500 ns, and we did not take reaction 9 into account. Without it, the signals of Figure 6 cannot be fitted satisfactorily, and the abovementioned crossing of the two decays around 800 ns cannot be simulated.

We also introduce reaction 10 to take care of a hypothetical spontaneous decay pathway that will be discussed in section 3.2.4.

$$P \rightarrow P' \qquad (10)$$

We will discuss below the nature of P and P′.

The kinetics model for a single signal includes 10 parameters—extinction coefficients $\epsilon_{e_s^-}$, ϵ_P, and $\epsilon_{P'}$; rate constants k_1, k_7, k_9, k_{10}; and initial concentrations $[e_s^-]_0$, $[THF^+]_0$, and $[Mg^{II}]_0$—seven of which are totally unknown (ϵ_P, $\epsilon_{P'}$, k_1, k_9, k_{10}, $[e_s^-]_0$, and $[THF^+]_0$) and to which we assign log-uniform prior pdf's (Table 2). We transfer the posterior pdf's obtained in the analysis of pure THF (section 2.1) as prior pdf's for $\epsilon_{e_s^-}$ and k_7. A preliminary analysis showed that the value of the extinction coefficient of P′ must be zero. A global analysis of the set of 6 transient signals reported in Figure 6, with the model including the whole set of 19 parameters, revealed identifiability problems, preventing the MCMC procedure from converging in an acceptable run length. This behavior has been traced back to strong correlations of certain parameters with $\epsilon_{e_s^-}$ and k_7. To overcome this difficulty, we fixed $\epsilon_{e_s^-}$ and k_7 to their optimal values, obtained in section 2.1 ($\epsilon_{e_s^-} = 10^4$ mol^{-1} dm^3 cm^{-1}, $k_7 = 1.9 \times 10^{12}$ mol^{-1} dm^3 s^{-1}). Under these conditions, the model is identifiable (see Figure 7 and Table 2). The marginal posterior pdf of k_{10} is almost identical to its prior pdf, but k_{10} has a vanishing probability to be greater than 10^5 s^{-1}. The residues for the best fit of the observed kinetics with this set of parameters are given on the top panel of Figure 6. They show that the fits are very good.

As an example, the time evolutions of the concentrations of the solvated electron P and P′ are given in the Figure 6 inset for $[Mg^{II}] = 5 \times 10^{-3}$ mol dm^{-3}, $k_1 = 6.2 \times 10^9$ mol^{-1} dm^3 s^{-1}, $k_9 = 3.8 \times 10^6$ s^{-1}, and $k_{10} = 10^5$ s^{-1}. The very fast decay of the solvated electron is correlated to the formation of P and

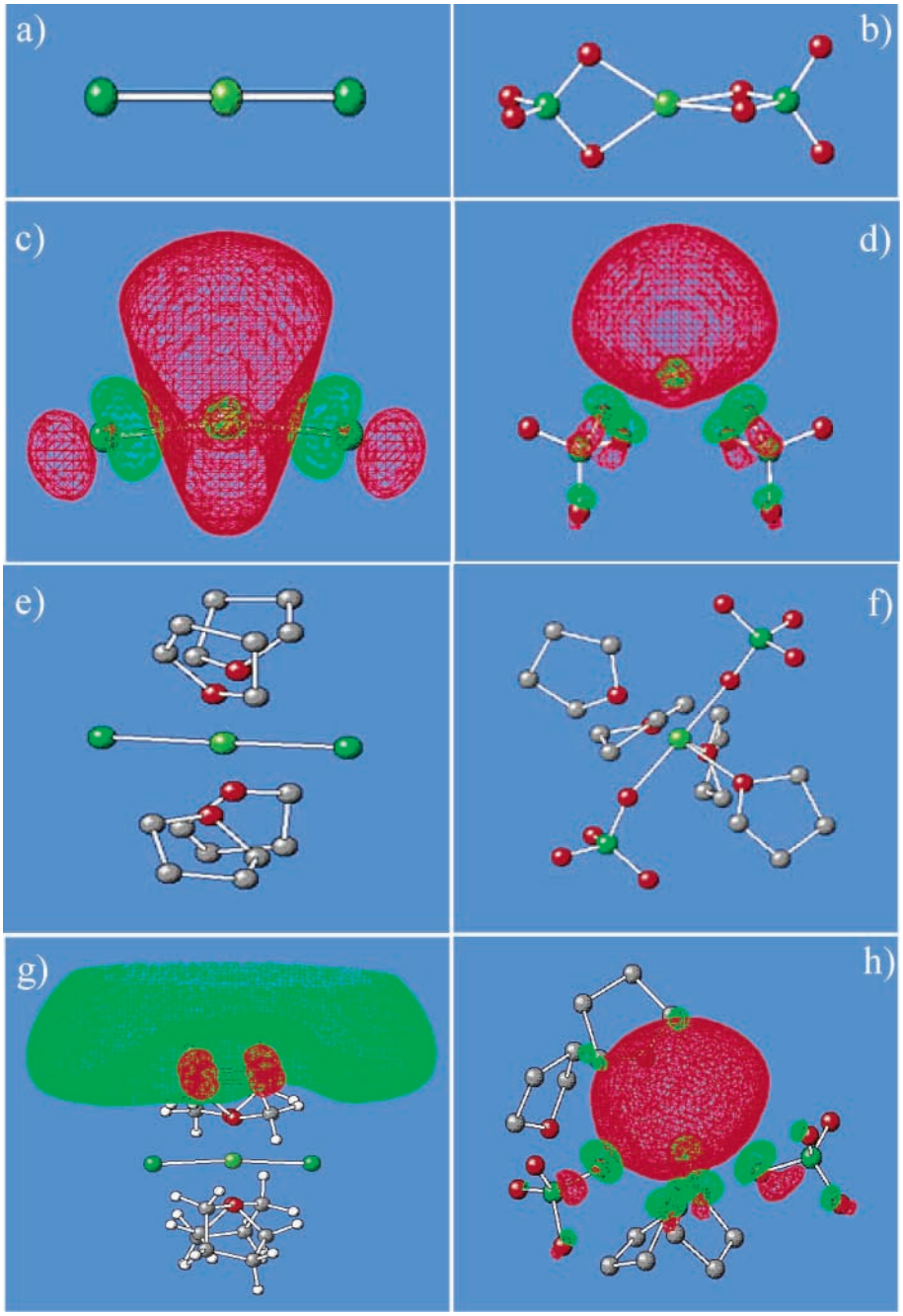

Figure 8. Optimized structure in the gas phase with the SCF method of (a) $MgCl_2$, (b) $Mg(ClO_4)_2$, (c) $MgCl_2^-$, (d) $Mg(ClO_4)_2^-$, (e) $MgCl_2$, (f) $Mg(ClO_4)_2$, (g) $MgCl_2^-$, and (h) $Mg(ClO_4)_2^-$.

also to the reaction with THF^+ (reaction 7). The product of reaction 1 reaches a maximum 50 ns after the pulse and decays slowly. The maximum of the P concentration is slightly above 5×10^{-6} mol dm^{-3} for an initial concentration of the solvated electron of about 8.5×10^{-6} mol dm^{-3}.

We remark that even for the upper-limit value of $k_{10} = 10^5$ s^{-1} the concentration of P′ formed through reaction 10 is very low and can be neglected. Although there is no experimental evidence for the formation of P′ under our conditions, we discuss the possible formation of P′ in section 3.2.4.

The sensitivity of the global parameters to $\epsilon_{e_s^-}$ and k_7 has been evaluated by performing two additional analyses, with $\epsilon_{e_s^-}$ at the limits of its range and k_7 chosen at its optimum, given $\epsilon_{e_s^-}$ (see Table 2). Rate constants k_1 and k_9 are well defined and are almost insensitive to changes in $\epsilon_{e_s^-}$. In contrast, one can also see from Table 2 that the recovered value of ϵ_P is significantly correlated to the chosen value of $\epsilon_{e_s^-}$. Given the uncertainty in $\epsilon_{e_s^-}$, we estimate that $\epsilon_P = (4.0 \pm 0.4) \times 10^4$ mol^{-1} dm^3 cm^{-1}.

3. ab Initio Investigation of Electron Attachment on $MgCl_2$ and $Mg(ClO_4)_2$. Electronic ab initio calculations have been undertaken to elucidate the structure of the product of reaction 1 and to explain the difference in reactivity of the solvated electron with $Mg(ClO_4)_2$ and $MgCl_2$.

3.1. Structure of $MgCl_2$ and $Mg(ClO_4)_2$ and of Their Negative Ions in the Gas Phase. The SCF optimized structures of gas-phase $MgCl_2$ and $Mg(ClO_4)_2$ and their anions are displayed in Figure 8a−d. The isodensity surface of the HOMO (highest occupied molecular orbital) for the anions is also shown in Figure 8c and d. It can be seen that the neutrals $MgCl_2$ (Figure 8a) and $Mg(ClO_4)_2$ (Figure 8b) are highly symmetrical and that, conversely, the two anions display a bending of the ClMgCl

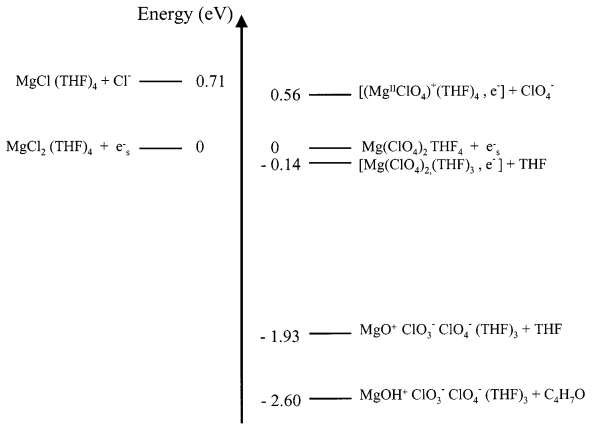

Figure 9. Energy diagram for the different species involved in reactions 1, 9, and 10 calculated by the DFT/Onsager method including the solvation energy of the solvated electron.

angle (Figure 8c and d). We have found that the structure and the stability of MgX_2^- strongly depend on the nature of the anion X^-:

• In the case of $MgCl_2^-$, the ClMgCl bending is weak, only 12° (Figure 8c). This value reflects the weak electron affinity of $MgCl_2$: 0.23 eV at the SCF level. The HOMO of $MgCl_2^-$ displays very diffuse character, with a coefficient of 0.26 on its most diffuse s Gaussian, of exponent 0.01. Figure 8c shows that this HOMO overlaps the whole nuclear structure, except the repulsive anionic zone, with a slight preference for one side of the cation.

• In the case of $Mg(ClO_4)_2^-$, the ClMgCl bending is much larger (70°, Figure 8d), reflecting the large electron affinity of $Mg(ClO_4)_2$: 1.14 eV at the SCF level. The HOMO of $Mg(ClO_4)_2^-$ is much less diffuse than that of $MgCl_2^-$: it displays a coefficient of 0.13 on its must diffuse s Gaussian, of exponent 0.02. It can be seen in Figure 8d that this HOMO is strongly localized on one side of the molecule, even looking like an s orbital, located beside the metal cation. The additional electron thus behaves like a ligand, forming what we will call hereafter the molecule/electron pair [$Mg(ClO_4)_2$, e^-].

The different influences of chloride and perchlorate counterions can be qualitatively understood with the help of the Mulliken charges of the neutrals. In the case of $MgCl_2$, the incoming electron encounters a compact $Cl^{-.35}-Mg^{+.70}-Cl^{-.35}$ structure, and in the case of $Mg(ClO_4)_2$, it sees a much more extended and complex structure: $(O^{-0.56})_2-Cl^{+2.1}-(O^{-0.77})_2-Mg^{+1.2}-(O^{-0.77})_2-Cl^{+2.1}-(O^{-0.56})_2$. In the latter case, the positive charges are larger and more numerous, which is probably the determinant for the binding of the additional electron.

A similar strong polarization of Mg^+ by ligands has already been noticed in the literature, as, for instance, in the study of $(Mg(H_2O)_n)^+$ clusters,[38] where structures very similar to the [$Mg^{2+}H_2O$, e^-] and [Mg^{2+} $(H_2O)_2$, e^-] pairs are reported. The investigation of the free solutes in vacuum is thus already very informative: it shows that Mg^+ is very unlikely to exist as such in an environment of ligands.

3.2. Solutes and Their Anions in THF. We now consider the two solutes surrounded by a few THF molecules, with the remaining solvent treated like a continuum. Figure 9 displays the energy levels of the neutrals and negative ions at the DFT/Onsager level, including the solvation energy of the electron in THF (see below).

3.2.1. Case of Magnesium Chloride. It is known that the first solvation shell of magnesium chloride in THF contains four THF molecules.[39] Neutral $MgCl_2(THF)_4$ displays a typical octaedric structure, as can be seen in Figure 8e, with the four THFs orienting their dipoles toward the metal cation, as expected. Adding one electron to the system generates two structures of interest:

• A dissociated $MgCl(THF)_4 + Cl^-$ structure. Separate calculations for $MgCl(THF)_4$ and Cl^- yielded the result that this channel lies 0.21 eV under $MgCl_2(THF)_4$ at the DFT/Onsager level. The HOMO is diffuse and located beside the solute, indicating that this species is the [$MgCl(THF)_4^+$, e^-] pair.

• A very diffuse species, lying 0.65 eV above $MgCl_2(THF)_4$ at the gas-phase SCF level. This species has actually no physical meaning because its outer electron is not bound: adding more and more diffuse Gaussians to the basis set results in an electron escaping to infinity and in the energy of the anion tending to that of the neutral. The structure of this nonphysical [$MgCl_2(THF)_4$]$^-$ state and the shape of its diffuse orbital are shown in Figure 8g, for comparison with perchlorate. This species is not reported in Figure 9.

We have not succeeded in building a stable [$MgCl_2(THF)_4$, e^-] pair; we therefore conclude that this species probably does not exist in THF.

3.2.2. Case of Magnesium Perchlorate. We have optimized the gas-phase structures of $Mg(ClO_4)_2$ with 2, 3, and 4 THF molecules and have found that the environment of magnesium is always octaedric. This is due to the fact that each perchlorate can be mono- or bidentate: in $Mg(ClO_4)_2(THF)_4$, each of the perchlorates is monodentate (Figure 8f), but dropping one THF first and then a second one provokes a rearrangement with one perchlorate first and then the second one becoming bidentate. Perchlorate is thus a very adaptable ligand, tending to fill the coordination shell of magnesium to six when other ligands are missing. Such a coordination has already been reported for $Mg(ClO_4)_2$ in acetonitrile.[40] The formation of the pair is very similar in all of the studied cases: at the SCF level in the gas phase, it is endothermic by 0.7, 1.2, and 1.2 eV when 2, 3, and 4 THF are present, respectively. In every case, the formation of the pair provokes a rearrangement of the solute, with all ligands mainly gathered on one-half of the available space and the electron on the other side. If two or three THF molecules are present, then this rearrangement is enabled by one ClO_4^- passing from bidentate to monodentate. If four THF molecules are present, then this rearrangement is enabled by the departure of one THF. At the DFT/Onsager level, the rearrangement becomes exothermic in all cases.

We now further discuss the case with four THF ligands. The optimization of $Mg(ClO_4)_2(THF)_4^-$ yields the following structures:

(1) A solute/electron pair, [$Mg(ClO_4)_2(THF)_4$, e^-], in which one THF is moved aside (Figure 8h). The structure of this pair is similar to that of $Mg(ClO_4)_2^-$, with a smaller ClMgCl bending angle of 45°. Separate calculations were carried out on [$Mg(ClO_4)_2(THF)_3$, e^-] and on one THF molecule. With this method, we show that this channel lies 1.06 eV below the neutral at the DFT/Onsager level.

(2) A dissociated [$MgClO_4(THF)_4^+$, e^-] + ClO_4^- structure. The separate calculation of [$MgClO_4(THF)_4^+$, e^-] and ClO_4^- yielded the result that this channel lies 0.36 eV below the neutral at the DFT/Onsager level. The departure of one perchlorate is thus possible but less favorable than that of one THF.

(3) A nonphysical diffuse species with an unbound electron as in the case of [$MgCl_2(THF)_4$]$^-$.

These results suggest that electron scavenging can initiate the departure of one ligand, THF or ClO_4^-, but to be able to

reach conclusions on the thermodynamics of these pathways in solution, we need to evaluate the solvation free energy of the electron in THF.

3.2.3. Thermodynamics of Pair Formation. The solvation free energy of the electron in THF is not available in the literature. Therefore, we evaluate it from its value in water (1.7 eV)[41] and from the Born model. In this model, the solvation free energy strongly depends on the charge of the solute (q), on the cavity radius (R), and more weakly on ϵ, the dielectric constant of the solvent:

$$\Delta G_{solv} = -(q^2/2R)(1 - 1/\epsilon) \quad (11)$$

Considering the values of the dielectric constant of water (78) and THF (7.6) and the fact that the cavity radius of the solvated electron has been evaluated to be 3.4 Å in THF and 2 Å in water,[42,43] the solvation free energies of the electron in water and in THF should be in a ratio of roughly 1.9. This yields an approximate value of 0.9 eV for the solvation free energy of the electron in THF.

If we use this value and the energies obtained in sections 3.2.1 and 3.2.2 for the departure of one THF, we find the following reaction free enthalpy:

$$e_s^- + Mg(ClO_4)_2(THF)_4 \rightarrow [Mg(ClO_4)_2(THF)_3, e^-] + THF \qquad \Delta G = -0.16 \text{ eV} \quad (12)$$

In section 2, we have determined the values of the rate constants for the formation and dissociation of the pair (reactions 1 and 9). The corresponding equilibrium constant ($K = k_1/k_9 = 1630 \pm 50$ mol^{-1} dm^3) gives a free enthalpy of -0.18 ± 0.01 eV for the formation of the pair, in good agreement with the ab initio value (-0.16 eV).

In the case of the departure of one perchlorate ligand, we obtain

$$e_s^- + Mg(ClO_4)_2(THF)_4 \rightarrow [MgClO_4^+(THF)_4, e^-] + ClO_4^- \qquad \Delta G = +0.54 \text{ eV} \quad (13)$$

We can also evaluate the free-energy variation for the equivalent of reaction 13 for $MgCl_2$:

$$e_s^- + MgCl_2(THF)_4 \rightarrow (MgCl^+(THF)_4, e^-) + Cl^- \qquad \Delta G = +0.71 \text{ eV} \quad (14)$$

The formation of the pair is thus endothermic for both solutes if a counterion is released, and it can only be exothermic in the case of perchlorate through the release of one THF. More accurate calculations are in progress and will be discussed in a forthcoming paper.[44]

3.2.4. Product of the Decay of the Pair. The kinetics models (section 2) show that the decay of the $[Mg(ClO_4)_2(THF)_3, e^-]$ pair is mostly due to its dissociation through reaction 9. Our ab initio calculations reveal an alternative pathway for the decay of the pair (reaction 10) through internal reduction:

$$[Mg(ClO_4)_2(THF)_3, e^-] \rightarrow MgO^+ClO_3^-ClO_4^-(THF)_3 \quad (15)$$

This reaction is exothermic by 1.8 eV at the DFT/Onsager level. Actually, MgO^+ has the structure of $Mg^{2+}O^-$, showing that reaction 15 is actually a reduction of one perchlorate to chlorate, catalyzed by Mg^{2+}. We have also found that this product can react with THF according to

$$MgO^+ClO_3^-ClO_4^-(THF)_4 + C_4H_8O \rightarrow MgOH^+ClO_3^-ClO_4^-(THF)_4 + C_4H_7O \quad (16)$$

This last reaction is exothermic by 0.7 eV at the DFT/Onsager level. The reduction of perchlorate to chlorate is very rare in water, the only known reducing agent being Ru^{II}.[45] Thus, we propose reactions 15 and 16 as hypotheses only, and probably other mechanisms are possible. According to the above ab initio calculations, the species P and P′ in reactions 1, 9, and 10 could be identified as $[Mg(ClO_4)_2(THF)_3, e^-]$ and $MgO^+ClO_3^-ClO_4^-(THF)_3$, respectively. But under our conditions, we did not observe the new pathway (reaction 10) for the decay of the pair. Therefore, the decomposition of the pair to P′ should be negligible.

Conclusions

From conductimetry measurements, we showed that the dissociation of $MgCl_2$ and $Mg(ClO_4)_2$ is negligible in THF and that they are solvated in their neutral forms. From pulse radiolysis measurements, we observed a reaction of the solvated electron with magnesium perchlorate only, leading to a product absorbing light in the near-infrared. Ab initio calculations showed that the product of this reaction is the pair $[Mg(ClO_4)_2(THF)_3, e^-]$ and that such a pair cannot be formed with $MgCl_2$. The geometry of the magnesium perchlorate has been found to change when the solvated electron is in the vicinity of the magnesium cation. As we observed, the rate constant of ion pairing with magnesium ions (reaction 1) is 2 orders of magnitude below the diffusion limit. That can be explained by the presence of a kinetic barrier for the formation of the ion pair. In fact, the structure around Mg^{II} has to be modified markedly when an electron comes close to magnesium. Because THF is a low dielectric medium, the magnesium ions have a strong interaction with the perchlorate ions, but this interaction does not favor the reaction with the solvated electron. Theoretical calculations suggest that the pair formation is accompanied by the departure of one THF ligand. The $[Mg(ClO_4)_2(THF)_3, e^-]$ pair lasts only a few hundreds of nanoseconds in THF.

Monovalent magnesium, if we identify it with the pair (e_s^-, Mg^{II}), can be considered to be a reducing species in solution. This property should be taken into account if under certain conditions Mg^I is produced in a solvent such THF, for example, during the formation of Grignard compounds (RMgX). In the second part of this work, we will show the results of the reactivity of the pair toward different organic molecules.

The nature of the absorption spectrum of the pair will be discussed in a future paper. It is interesting that this absorption spectrum presents an important blue shift and displays two maxima, in contrast to other pairs with alkaline metals in THF. This feature could be due to a splitting of the p state of the solvated electron that is caused by a strong interaction with the double positive charge of Mg^{II}. Experimental and theoretical work is in progress to elucidate this important result.

Appendix: Bayesian Data Analysis

The probabilistic or Bayesian approach to data analysis has been extensively detailed by other authors.[15−18] Currently, maybe because of the lack of dedicated black box programs, this method has not yet been put to extensive use in chemical kinetics analysis. Notwithstanding, our experience with it in this field reveals very interesting aspects, essentially when identi-

fiability issues are considered.[46] We provide here a brief summary of the basic concepts and details of its actual implementation.

We consider a general framework, where we attempt to identify a set of parameters u from the analysis of a set of data D. Parameters and data are related through a (kinetic) model that is considered here to be optimal (i.e., this model has been selected beforehand).

A1. Principles. The central object of probabilistic data analysis is the so-called posterior probability density function (pdf) of u conditional to D, noted $p(u|D)$. This distribution expresses the uncertainties of the value of the parameters resulting from the measurement uncertainties of the data set. It contains all of the sought after information on the parameters, and it is generally used to obtain estimates of the functions of the parameters

$$E[f(u)] = \int \mathrm{d}u\, f(u)\, p(u|D)$$

where the integral runs over all parameter space. For instance, the mean value of an individual parameter, u_i, is obtained through

$$E[u_i] = \int \mathrm{d}u\, u_i\, p(u|D)$$

Of particular interest are the so-called marginal densities for individual parameters

$$p(u_i|D) = \int \mathrm{d}u_{-i}\, p(u|D)$$

where $\mathrm{d}u_{-i}$ means that the integration is performed on all parameters except u_i. This function gives the posterior distribution of a parameter "averaged" over all of the possible values of the other parameters. Similarly, marginal densities for pairs of parameters can be calculated:

$$p(u_i, u_j|D) = \int \mathrm{d}u_{-i,-j}\, p(u|D)$$

These contain essential information on the couplings between pairs of parameters, and they are of diagnostic relevance for identifiability studies.

A2. Bayesian Inference. To express the posterior pdf, we need to relate it to computable quantities through Bayes' rule

$$p(u|D) \propto p(D|u)\, p(u)$$

where $p(D|u)$ is the likelihood (probability of observing dataset D at a given point in parameters space) and $p(u)$ is the prior pdf, based on the information on the parameters before the analysis of dataset D. Bayes' rule thus provides an inference method for the parameters.

A2.a. Likelihood. The likelihood $p(D|u)$ is obtained by assigning a probability law to the measured data, taking into account measurement uncertainties. For the present work, we consider uncorrelated, homoscedastic, additive, normally distributed uncertainties. The variance of the noise being a priori unknown, we assign it a log-uniform prior pdf $p(\sigma)$ (cf. below) and eliminate it by integration

$$p(D|u) = \int \mathrm{d}\sigma\, p(\sigma)\, p(D|u, \sigma) \propto (\chi^2)^{-m/2}$$

where χ^2 is the sum of the squares of residuals between the model and the m analyzed data.[15]

A2.b. Prior pdf. The prior pdf $p(u)$ enables us to take a priori knowledge of the parameters into account in a consistent way (including parameter transfer during the analysis of successive data sets). Its functional form depends on the available information. For instance, if all we know is that parameter u_i belongs to an interval, $u_i \in$ [a, b], then we might assign it a uniform distribution

$$p(u_i) = 1/(\mathrm{b} - \mathrm{a}) \text{ inside [a, b]} \qquad p(u_i) = 0 \text{ elsewhere}$$

When the scale of a positive parameter is not known, it is better to use a log-uniform distribution:

$$p(u_i) = 1/(u_i \log(\mathrm{b/a})) \text{ inside [a, b]}$$

$$p(u_i) = 0 \text{ elsewhere}$$

We consistently use this log-uniform prior throughout the present work. Another very common case occurs when we know the mean value μ and standard deviation σ for a parameter. It is then customary (and justified by the maximum entropy principle) to assign the parameter a normal distribution of $\mathcal{N}(\mu, \sigma^2)$.

If the parameters are independent, then the total prior pdf is the product of prior pdf's for the individual parameters; otherwise, correlated priors have to be used.

A3. Markov Chain Monte Carlo. For models based on more than five or six parameters, the multidimensional integrals involved in estimates or marginal distribution computations cannot generally be performed by grid methods. Instead, one has to use stochastic integration. The Markov chain Monte Carlo (MCMC) method has proven to be quite efficient in this context.[23−25] We use the Metropolis−Hastings algorithm to perform random walks in parameter space. Once the chain has reached equilibrium, the samples are used to calculate the marginal posterior distributions for the parameters and to estimate their mean values and standard deviations (if meaningful). In the case of an unidentifiable model, even a nonconverged chain can provide insight into the problem. A visual inspection of scatter plots for pairs of parameters reveals correlation patterns and identifiability problems, suggesting possible solutions (e.g., reparametrizing the model).

A4. Practical Implementation. The practical procedure we apply is the following:

(1) Define a kinetic model and prior distribution $p(u)$.

(2) Test this model by searching $\hat{u}$, the mode of $p(u|D)$ in parameter space. We run multiple local searches from randomly generated starting points inside the prior's range; the localization of multiple modes of the posterior is diagnostic for identification.

(3) Accept or reject the model according to the quality of the fit at $\hat{u}$. If the model is satisfying, then proceed to the next step; otherwise, go back to step 1.

(4) A set of MCMC runs is performed for the chosen model, ensuring convergence.

(5) One- and two-parameter marginal pdf's are computed, and the corresponding density plots and scatter plots are visually inspected.

(6) Statistical summaries are finally issued for those parameters that are identified.

References and Notes

(1) Buxton, G. V.; Greenstock, C. L.; Helman, W. P.; Ross, A. B. *J. Phys. Chem. Ref. Data* **1988**, 17. Buxton, G. V.; Mulazzani, Q. G.; Ross, A. B. *J. Phys. Chem. Ref. Data* **1995**, 24.

(2) Bockrath, B.; Dorfman, L. M. *J. Phys. Chem.* **1973**, *77*, 1002. Fletcher, J. W.; Seddon, W. A. *J. Phys. Chem.* **1975**, *79*, 3055.

(3) Hickel, B. *J. Phys. Chem.* **1978**, *82*, 1005.

(4) Hart, E. J.; Anbar, M. *The Hydrated Electron*; Wiley-Interscience: New York, 1970. Anbar, M.; Meyerstein, D. *J. Phys. Chem.* **1964**, *68*, 1713.

(5) Renou, F.; Mostafavi, M. *Chem. Phys. Lett*. **2001**, *335*, 363.
(6) Bram, G.; Péralez, E.; Negrel, J. C.; Chanon, M. *C. R. Acad. Sci.,, Sér. IIb* **1997**, 235.
(7) Bickelhaupt, F. *J. Organomet. Chem*. **1994**, *1*, 475.
(8) Garst, J.; Hungvary, F. In *Grignard Reagents: New Developments;* Richey, H. G., Ed.; Wiley: New York, 2000.
(9) Belloni, J.; Billiau, F.; Cordier, P.; Delaire, J.; Delcourt, M. O. *J. Phys. Chem.* **1978**, *82*, 532.
(10) Petzold, L. R. *Siam J. Sci. Stat. Comput.* **1983**, *4*, 136.
(11) Bonneau, R.; Wirz, J.; Zuberbühler, A. D. *Pure Appl. Chem.* **1997**, *69*, 979.
(12) Vajda, S.; Rabitz, H. *J. Phys. Chem.* **1988**, *92*, 701. Vajda, S.; Rabitz, H. *J. Phys. Chem.* **1994**, *98*, 5265.
(13) Walter, E.; Pronzato, L. *Identification of Parametric Models from Experimental Data;* Springer: New York, 1997.
(14) Beechem, J. M.; Ameloot, M.; Brand, L. *Chem. Phys. Lett*. **1985**, *120*, 466.
(15) Sivia, D. S. *Data Analysis: A Bayesian Tutorial;* Clarendon: Oxford, U.K., 1996.
(16) Gelman, A.; Carlin, J. B.; Stern, H. S.; Rubin, D. B. *Bayesian Data Analysis;* Chapman & Hall: London, 1995.
(17) D'Agostini, G. *Bayesian Reasoning in High Energy Physics: Principles and Applications;* Technical Report 99-03; CERN, Geneva, July 1999.
(18) Ó Ruanaidh, J. J. K.; Fitzgerald, W. J. *Numerical Bayesian Methods Applied to Signal Processing;* Springer: New York, 1996.
(19) Schwartz-Selinger, T.; Preuss, R.; Dose, V.; Von der Linden, W. *J. Mass Spectrosc.* **2001** *36*, 866−874.
(20) Brun, R.; Reichert, P.; Kunsch, H. R. *Water Resour. Res.* **2001**, *37*, 1015.
(21) D'Avignon, D. A.; Bretthorst, G. L.; Holtzer, M. E.; Holtzer. A. *Biophys. J.* **1988**, *74*, 3190. D'Avignon, D. A.; Bretthorst, G. L.; Holtzer, M. E.; Holtzer. A. *Biophys. J.* **1999**, *76*, 2752.
(22) Holtzer, M. E.; Bretthorst, G. L.; D'Avignon, D. A.; Angeletti, R. H.; Mints, L.; Holtzer, A. *Biophys. J.* **2001**, *80*, 939.
(23) Gilks, W. R.; Richardson, S.; Spiegelhalter, D. J. *Markov Chain Monte Carlo in Practice;* Chapman & Hall: London, 1996.
(24) Chen, M.-H.; Shao, Q.-M.; Ibrahim, J. G. *Monte Carlo Methods in Bayesian Computation;* Springer: New York, 2000.
(25) Robert, C. P.; Casella, G. *Monte Carlo Statistical Methods*; Springer: New York, 1999.
(26) Frisch, M. J.; Trucks, G. W.; Schlegel, H. B.; Scuseria, G. E.; Robb, M. A.; Cheeseman, J. R.; Zakrzewski, V. G.; Montgomery, J. A., Jr.; Stratmann, R. E.; Burant, J. C.; Dapprich, S.; Millam, J. M.; Daniels, A. D.; Kudin, K. N.; Strain, M. C.; Farkas, O.; Tomasi, J.; Barone, V.; Cossi, M.; Cammi, R.; Mennucci, B.; Pomelli, C.; Adamo, C.; Clifford, S.; Ochterski, J.; Petersson, G. A.; Ayala, P. Y.; Cui, Q.; Morokuma, K.; Malick, D. K.; Rabuck, A. D.; Raghavachari, K.; Foresman, J. B.; Cioslowski, J.; Ortiz, J. V.; Stefanov, B. B.; Liu, G.; Liashenko, A.; Piskorz, P.; Komaromi, I.; Gomperts, R.; Martin, R. L.; Fox, D. J.; Keith, T.; Al-Laham, M. A.; Peng, C. Y.; Nanayakkara, A.; Gonzalez, C.; Challacombe, M.; Gill, P. M. W.; Johnson, B. G.; Chen, W.; Wong, M. W.; Andres, J. L.; Head-Gordon, M.; Replogle, E. S.; Pople, J. A. *Gaussian 98*; Gaussian, Inc.: Pittsburgh, PA, 1998.
(27) Makarenko, B. K.; Mendzheritskii, E. A.; Sobolev, R. P.; Povarov, Y. M. *Elektrokhimiya* **1974**, *10*, 355.
(28) De Groof, B.; De Smedt, C.; Vankerckhoven, H.; Van Beylen, M. *Bull. Soc. Chim. Belg.* **1990**, *99*, 1065.
(29) Fuoss, R. M.; Kraus, C. A. *J. Am. Chem. Soc.* **1933**, *55*, 2387.
(30) Micheletti, C. *Elargissement vers les Milieux de Basses Constantes Diélectriques du Domaine d'Application de la Conductibilité, à l'Etude des Solutions Electrolytiques Diluées*. Thesis, Pierre et Marie Curie, Paris, France, 1972.
(31) Farber, H.; Petrucci, S. *J. Phys. Chem.* **1976**, *80*, 327.
(32) Sigvartsen, T.; Gestblom, B.; Noreland, E.; Songstad, J. *Acta Chem. Scand.* **1989**, *43*, 103.
(33) Jagodzinski, P.; Petrucci, S. *J. Phys. Chem.* **1974**, *78*, 917.
(34) Bjerrum, N. *K. Dan. Vidensk Selsk. Mat.—Fys. Skr*. **1926**, *7*, 1. Fuoss, R. M.; Kraus, C. A. *J. Am. Chem. Soc.* **1933**, *55*, 476. Trémillon, B. *Electrochimie Analytique et Réactions en Solutions*; Masson: Paris, France, 1993.
(35) Salmon, G. A.; Seddon, W.; Fletcher, J. *Can. J. Chem.* **1974**, *52*, 3259.
(36) Andraos, J. *J. Chem. Educ.* **1999**, *76*, 1578.
(37) Dorfman, L. M.; Jou, F. Y.; Wageman, R. *Ber. Bunsen-Ges. Phys. Chem.* **1971**, *75*, 681.
(38) Bauschlicher, C. W.; Partridge H. *J. Phys. Chem.* **1991**, *95*, 9694.
(39) Handlir, K.; Holecek, J.; Benes, L. *Collect. Czech. Chem. Commun.* **1985**, *50*, 2422.
(40) Cha, J.-N.; Cheong, B.-S.; Cho, H.-G. *J. Phys. Chem. A* **2001**, *105*, 1789.
(41) Hickel, B. *Actions biologique et Chimiques des radiations ionisantes;* Tilquin, B., Ed.; Academia-Erasme: Louvin-la-Neuve, Belgium, 1992.
(42) Rossky, P. J.; Schnikter, J. *J. Phys. Chem.* **1988**, *92*, 4277. Schnikter, J.; Motakabbir, K.; Rossky, P. J.; Friesner, R. A. *Phys. Rev. Lett.* **1988**, *60*, 456.
(43) Martini, I. B.; Barthel, E. R.; Schwartz, B. J. *J. Chem. Phys.* **2000**, *113*, 11245.
(44) A more realistic mechanism for the formation of the pair actually involves two THF molecules.
(45) Cotton, F. A.; Wilkinson, G. *Advanced Inorganic Chemistry*, 5th ed.; Wiley: New York, 1988; p 568.
(46) Le Caër, S.; Henninger, M.; Pernot, P.; Mestdagh, H. *Phys. Chem. Chem. Phys.* **2002**, *4*, 1855.